Romanian Reports in Physics, Vol. 67, No. 2, P. 412–422, 2015

MEDICAL PHYSICS

CONTINUOUS WAWE DIFFUSE OPTICAL TOMOGRAPHY SYSTEM TESTED ON PHANTOMS AND ANIMAL TISSUES

M. PATACHIA, S. BANITA, C. POPA, D. C. DUMITRAS

National Institute for Laser, Plasma and Radiation Physics, Department of Lasers,
409 Atomistilor St., PO Box MG-36, 077125 Magurele, Ilfov,
E-mail: mihai.patachia@inflpr.ro

Received October 7, 2013

Abstract. Diffuse Optical Tomography (DOT) can image spatial variations in highly scattering optical media. We have built a continuous-wave DOT system containing a spatially combined 2 laser diode sources (at 785 nm and 830 nm), one SiPD detector, a transimpedance amplifier and two lock-in amplifiers, which can acquire 128 independent measurements in less than 60 seconds through two time-division-multiplexed optical scheme with eight illumination fibers and eight detector fibers in the measuring head (optode). These data can then be processed using a specialised imaging algorithm. We first discuss the design of diffuse imaging equipment in general, and then describe our instrument, along with the technical issues that influenced its design. The technical challenges involved in performing DOT over large optode areas are discussed. We also present the parametric evaluation of the system with an optode diameter of 5 to 6 cm. The paper describes the technique used to reach > 80 dB dynamic range, < 1% nonlinearity and a crosstalk < 0.01% at a digital resolution of 16 bits, how to put in evidence the selective absorption and scattering for some different kind of phantoms and their reconstructed images.

Key words: diffuse optical tomography, laser diode, multiplexer, phantom.

1. INTRODUCTION

Diffuse optical tomography (DOT) is a non-invasive technique used to measure the optical properties of physiological tissue. In the near-infrared (NIR) spectral window of 600 ÷ 1000 nm, photon propagation in tissues is dominated by scattering rather than absorption. Photons experience multiple scattering events as they propagate deeply into tissue (up to 10 cm). The primary chromophores in this spectral window are oxygenated hemoglobin (HbO2), deoxygenated hemoglobin (Hb), water (H2O) and lipids. Each chromophore possesses a distinct spectrum as shown in Fig. 1.

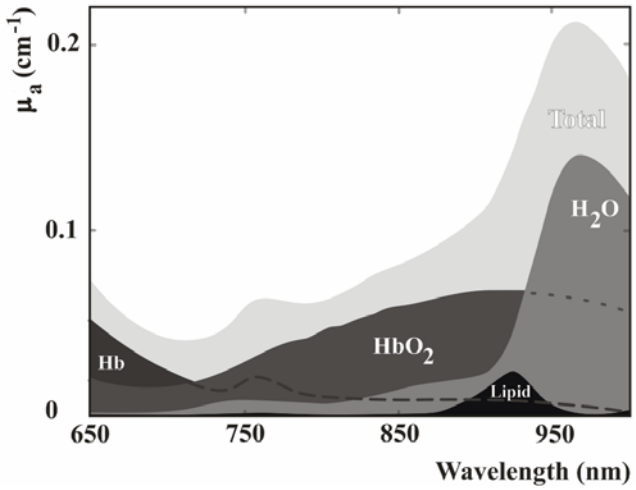

Fig. 1 – Absorption spectrum of the primary tissue constituents.

A weighted sum of the contributions from each chromophore which corresponds approximately to the tissue absorption coefficient (μa) is also shown. Here, the concentration of each chromophore is adjusted to a value typically found in breast tissue: the concentration of oxygenated hemoglobin (CHbO2) is ~ 24 μM, the concentration of deoxygenated hemoglobin (CHb) is ~ 6 μM, and the tissue is assumed to contain a 31% water and a 57% lipid contribution. This combination leads to total hemoglobin concentration, THC = CHb + CHbO2, of 30 μM, and a blood oxygen saturation, StO2 = CHbO2/THC, of ~ 80%. Notice that absorption measurements at multiple wavelengths are required to extract the concentration of each chromophore. Figure 2 shows typical scattering spectrum found in the breast tissue.

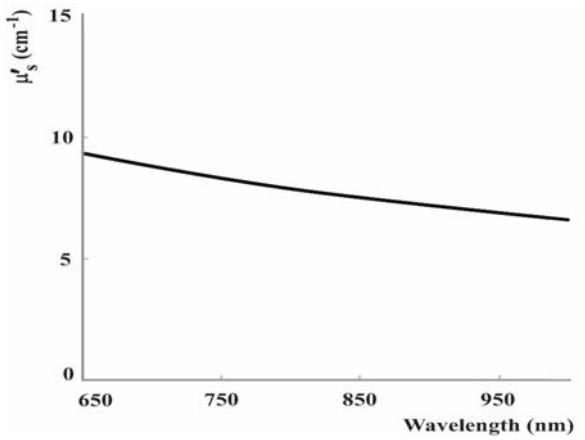

Fig. 2 – Typical reduced scattering coefficient of breast tissue.

The tissue scattering depends on the photon random walk step in the medium. The reduced scattering coefficient (μ´s), which is the reciprocal of the photon random walk step length, is often modelled within a simplified Mie-scattering approximation [1, 2], *i.e.* μ´s (λ) = $A\lambda^{-b}$, where λ is the light wavelength and *A* and *b* two specific coefficients of the turbid tissue media. For NIR radiations, the *A* coefficient is < 4. Notice that scattering is 100 times larger than the absorption and the NIR scattering spectrum is relatively flat in the near infrared.

Using optical measurements at multiple source-detector positions on the tissue surfaces, one can reconstruct the internal distribution of the absorption coefficient (μa) and the reduced scattering coefficient (μ´s) in two or three dimensions based on the transport model. Physiological images of total hemoglobin concentration, blood oxygenation, water and lipids are then derived from this information. Thus far DOT has generated a lot of scientific interest and has been applied in various deep-tissue applications including breast cancer imaging [3–7].

2. INSTRUMENT DESIGN

2.1. HARDWARE

We have built an inexpensive continuous-wave DOT system containing a spatially combined 2 laser diode sources RLT780-1000G (1 W at 785 nm) and RLT83500G (0.5 W at 830 nm) from Roithner Lasertechnik, a variable-gain photodetector OE-200-SI equipped with 1.2 mm active diameter Si photodiode and two lock-in amplifiers LIA-MV-150 from FEMTO Messtechnik GmbH, which can acquire 128 independent measurements in less than 45 seconds through two time-division-multiplexed optical scheme with eight illumination fibers and eight detector fibers in the measuring head (optode). The beams of the two laser diodes are collinearly overlaid and coupled into one of multiple source fiber bundles using an optical coupler Patchcord (RoMack Inc.) and four collimators two C230220P-B and two C220MP-B (ThorLabs Inc.). Switching between different sources is possible by means of an optical demultiplexer DMUX (single-input, multiple-output switch), which consists of a translation stage PI M505.2S2 (Mercury Inc.) which moves precisely the collimator in front of the illuminations fibers. The light transmitted through the target media (tissue phantom) is measured using a similarly serial approach realized with an optical multiplexer MUX (multiple-input, single-output switch) which moves precisely in front of the detecting fiber the collimator placed at the input of the photo preamplifier.

Each source/detector fiber bundle is fixed in a given order and alignment, on a mechanical mount placed in front of the illuminating/receiving collimator of the optical switches DMUX and MUX, respectively. A microprocessor-controlled stepper motor model M505.2S2 (20.000 counts/rev.) providing ultra-smooth, vibration free 0.1 μm minimum incremental motion, allows a relatively fast and precisely positioning of the collimator in front of the illumination/measuring fibers in a 50 mm travel range. The main set up of the DOT laboratory model is presented in Fig. 3.

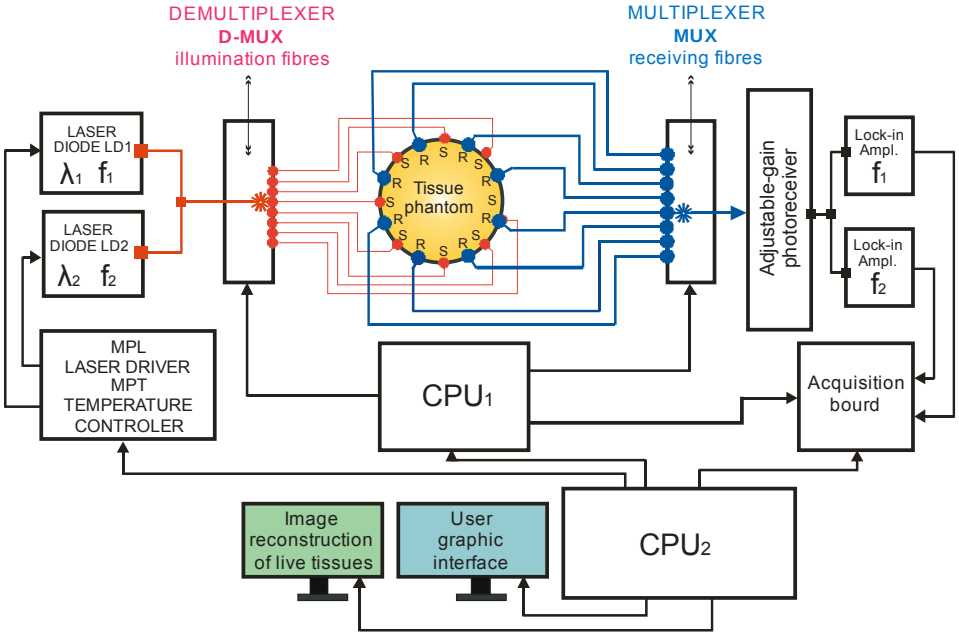

Fig. 3 – An overview of the DOT experimental setup.

Each source fiber bundle (0.225 mm diameter) from RoMack Inc. is placed radial and alternating with the receiving fibers in the measuring optode (Fig. 4).

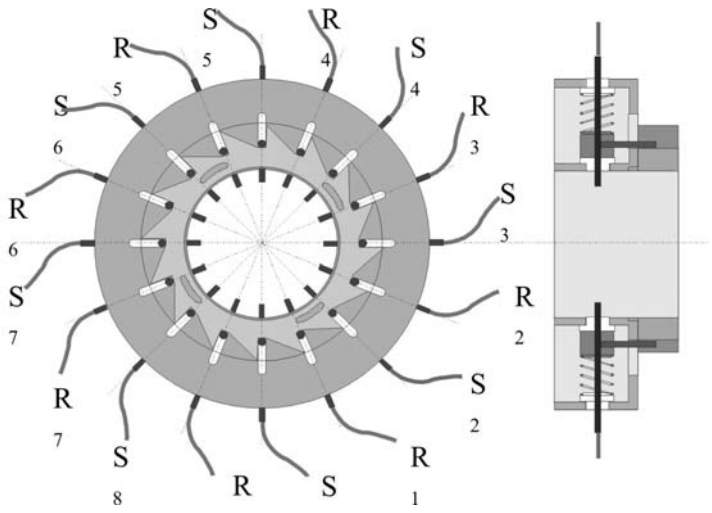

Fig. 4 – The optode and the radial distribution of the fiber bundle.

The microprocessor-equipped translation stages allow very flexible implementation of customized motion protocols. The Mercury II controller offers a high-

level mnemonic command language with macro compound command functionality. The unit is capable of performing ~ 64 start-stop motions per minute without noticeable errors.

2.2. DATA ACQUISITION

System operation is achieved through two levels of software control.

The first level is responsible for system timing and the second for data storage. The user interface in the first level is realized under MMCRun for Mercury Version 9.13 and in the second within a Keithley QuickDAQ environment.

The motor controller of the demultiplexer acts as the main clock for timing the various tasks such as advancing the source positions, performing the light detection, and acquiring/storing the data.

System complexity is proportional to the number of data channels, defined as WL × S × D, where WL represents the number of distinct near infrared source wavelengths (*e.g.*, WL = 2, namely 785 and 830 nm), S represents the number of source illumination fibers, and D represents the number of detector fibers in the measuring head.

The measuring head (optode) was built for simplicity with 8 illuminating fibers and 8 receiving fibers and with a measuring aperture of about 6 cm.

In order to obtain all the information available, each detector must be able of operating over 80 dB dynamic range, which is rather large from an electronic perspective. In order to collect enough photons to reach > 80 dB dynamic range, the laser power was increased at the maximum limit for tissue irradiation (about 30 mW) without vasodynamic effects of tissue heating and thermal necrosis and the detection noise was decreased to the limit of the fundamental uncertainty in the photon arrival rate. The detection of the measured light at the boundary of the illuminated tissue was realized with a monolithic adjustable-gain photoreceiver OE 200-IN (Femto). The OE-200 offers many more features than usual power meters, including selectable conversion gain from 103 to 1011 V/W, switchable AC/DC-coupling, and the capability of manual and opto-isolated remote control by a PC.

A picture of the waveforms monitored on the user interface is presented in Fig. 5. The collected data are available in four registration channels, two for the intensity measured at the boundary of the tissue (b, c) and two for the TTL signal (a, d) generated by the translation stages during the motion, to provide data viewing and analysis in real time.

A second CPU provides additional levels of data processing associated with image reconstruction, image display and image analysis. A variety of coupled forward-inverse reconstruction algorithms are available. They allow image recovery 2D or 3D using first-order or recursive finite element based scheme. Computed parameters include absorption only, scattering (diffusion) only, or both.

Fig. 5 – Data acquisition under QuickDAQ environment.

2.3. SYSTEM PERFORMANCE

The main characteristics of the diffuse optical tomography laboratory model realized in our group, are presented in Table 1.

Table 1

Main characteristics of the diffuse optical tomography laboratory model

DYNAMIC RANGE	10,000:1 (80dB)
NONLINEARITY	<1% over the 80dB dynamic range
SETTLING TIME	<300 ms to 0.1%
CROSSTALK	<0.01%
DIGITAL RESOLUTION	12 bits
SOURCE CHANNELS	8 at 785 nm and 8 at 830 nm
SOURCE OPTICAL POWER	~30 mW
DETECTORS	1 photoreceiver OE 200-IN (Si PIN Detector 1.2 mm active diameter, FC conector)
MODULATION	single-phase sinusoidal wave intensity modulation
POSTDETECTION BANDWIDTH	1 to 10Hz
STRAY LIGHT REJECTION	<1% error under normal illumination levels
POWER REQUIREMENTS	220 VAC +/-10%, 50Hz

2.4. EXTENSION OF DYNAMIC RANGE

The very large dynamic range of the signal, more than 80 dB require normally a 22 bit A/D converter and direct digitization. While such an A/D converter is not very common and is very expensive, we used the logarithmic compression and the gain control in the amplification stages to reduce the digital resolution of the A/D converter to 12 bits. We chose to use a 100 kilo sample-per-second, 12 bit A/D converter (KUSB-3102 - Keithley Inc. USA), because the high sample rate allowed us to rapidly scan through the 8 demodulated outputs and to use the oversample to average in the digital-domain and reduce consequently the noise limit.

The low-noise multi-stage amplifier design and the switchable 10 Hz low pass filter allow the precise measurements of low optical powers down to the 20 pW range without the need for further averaging. The measuring head was designed to operate within a normal hospital environment that means to have the ability to detect picowatts of source signal under an ambient optical background in the microwatt range (as seen by the detector). We solved this problem by using synchronous detection.

The acquisition board with a dynamic resolution of 12 bits enables in the measuring system a minimal detectable signal of 2.441 mV which correspond to a sensitivity of 107 V/W at an input power on the photodetector of about 200 pW. While the photodetector has equivalent noise input power of 20 pW, the 72 dB dynamic range of a normal acquisition board is limitative and the increase of the dynamic range to more than 80 dB need either the use of a 16 bits acquisition board, or the increase of the gain in the measuring system by 20 dB.

This last possibility need at least to measure cycles and the operation of the lock-in amplifier in overload region. Dynamic range and linearity are related: the dynamic range can only be defined with reference to a specified linearity limit. Long-term stability was measured by noting the total drift between initial and final readings for fixed probe geometry on a static phantom. Interchannel crosstalk was measured as a single detector channel and was alternately driven between the noise floor and full-scale output.

Stray light rejection was measured by operating the system with a static phantom in a dark room and then turning on both the fluorescent lights and a computer display located about a meter away. The largest change among the 8 detector channels was recorded. The detected power in the visible band was ~1.5 μW. This was not directly measured.

3. IMAGE RECONSTRUCTION FOR TISSUE PHANTOM AND ANIMAL TISSUE

To put in evidence the selective absorption of the hemoglobin at 785 nm, we investigated a liquid phantom (Fig. 6) made with 1% Lipofundin in a 50 mm diameter glass recipient and two thin 4 mm diameter glass tubes filled with diluted bovine hemoglobin.

In the case of the solid rubber phantom with a central metal bar immersed, with 16 mm diameter, the reconstruction algorithm has computed based on 128 measured values, the two coefficients for the opaque bar as being $\mu a = 0.023$ mm^{-1} and $\mu' s = 1.9$ mm^{-1}.

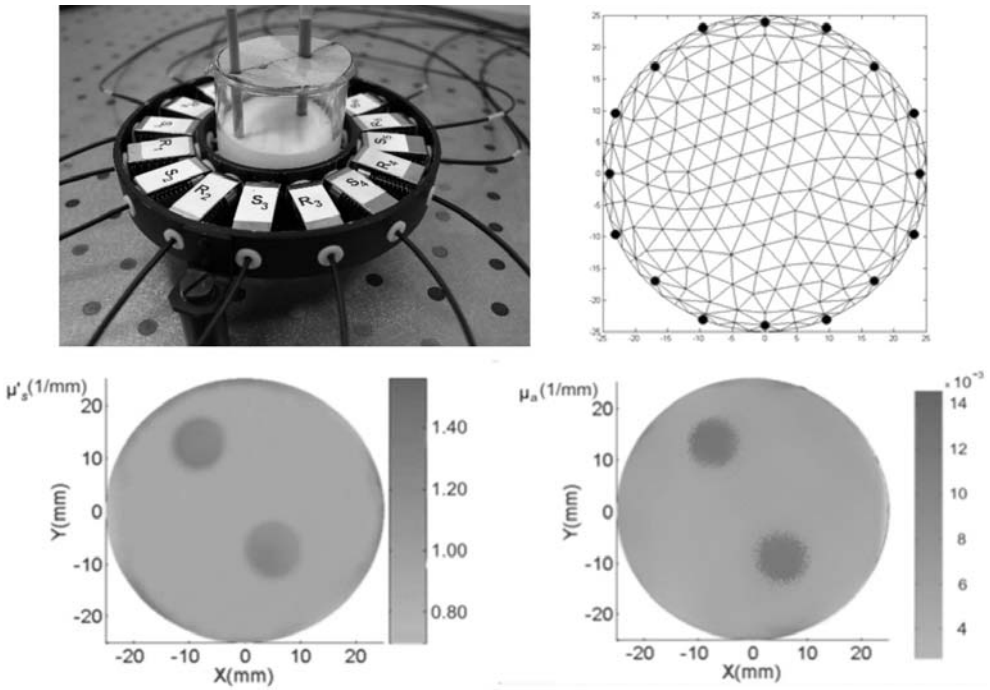

Fig. 6 – The liquid phantom with 1% Lipofundin and two glass tubes filled with hemoglobin.

The reconstruction algorithm has establish also the most probably XY distribution in the measuring plane for μa and μ´s taking into account 8.192 voxels for the substructure of the measuring plan. The image of the XY distribution of the μa and μ´s is presented in Fig. 7. The reconstruction image of the phantom structure is in good agreement with the measured probe.

For a lot test of the DOT setup, tissues collected from animals were used. Epithelized animal organs were selected, such as porcine tongue and kidney, containing specific chromophores of the breast in a similar proportion, such as: water, fat, hemoglobin, muscle, etc.

Where the size of the probes did not provide a uniform contact with the optical fibres, a glass-walled container of 1.5 mm and an outer diameter of 53 mm was used.

After measurements, the samples were sectioned to perform structural comparisons with representations of reconstruction program.

Figure 8 illustrates how the porcine kidney is fixed and reconstructed images, while Fig. 9 presents similar results for porcine tongue.

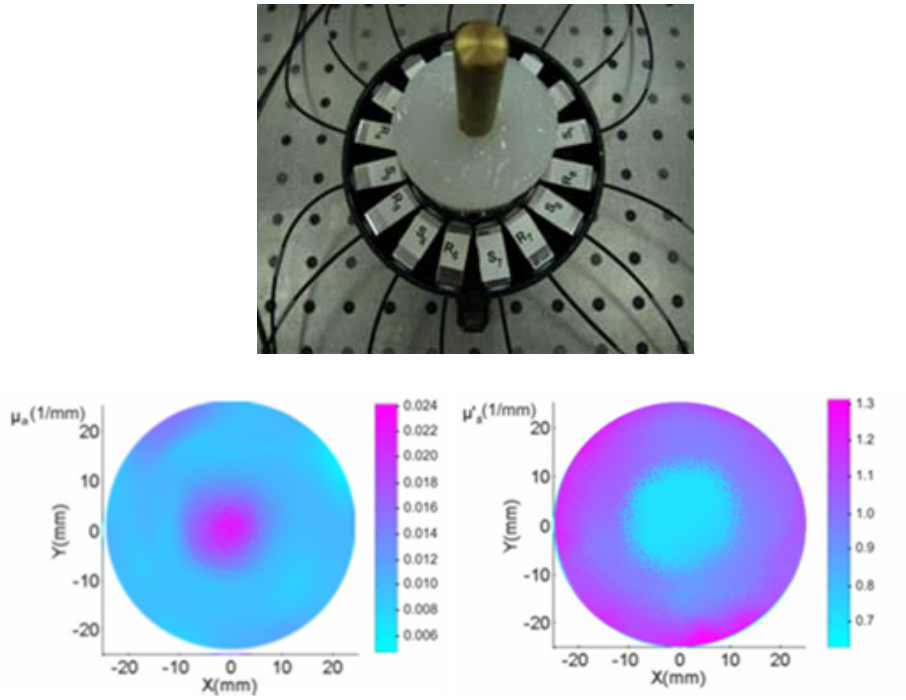

Fig. 7 – The rubber phantom with a central opaque metal bar.

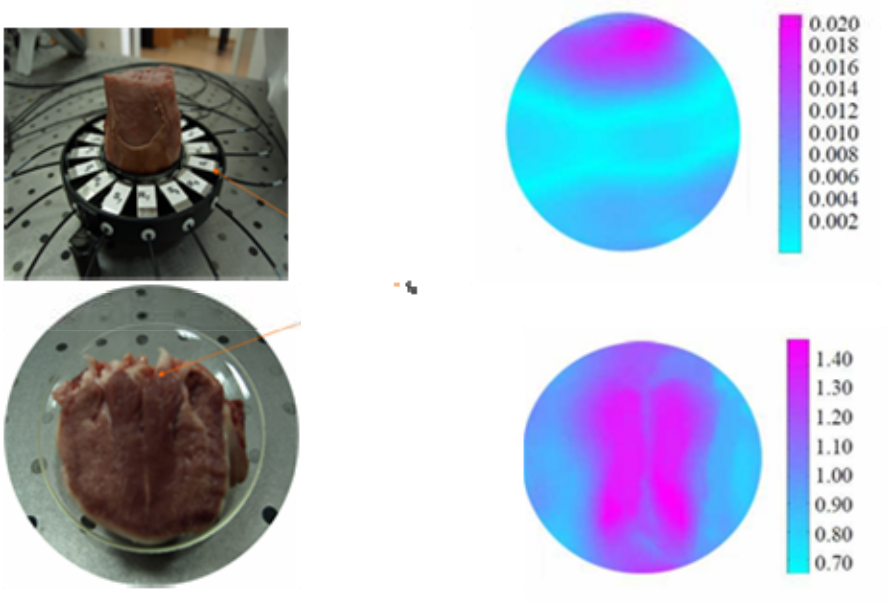

Fig. 8 – The porcine kidney sample and reconstructed images.

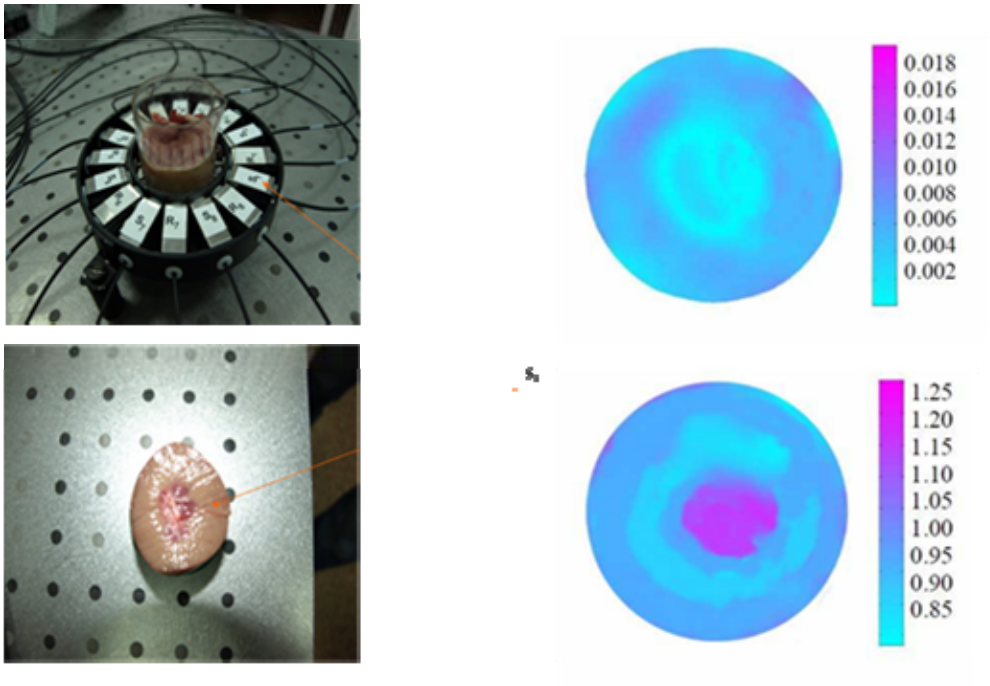

Fig. 9 – The porcine tongue sample and the reconstructed images.

4. CONCLUSIONS

To increase the reconstruction precision in the CW Diffuse Optical Tomography of turbid media, it is important to increase the number of the measuring data by increasing the number of the spectral sources used to illuminate the target, or to increase the number of the illuminating and measuring fibres. The best way of the CW imaging method needs however a special effort to solve the non-uniqueness problem of the method, which lacks the capability to separate absorption from scattering as in the Optical Tomography- OT image reconstruction.

To achieve this goal the CW imaging needs preconditioning and regularization techniques and multispectral laser sources.

In conclusion, we can highlight the following aspects: diffuse optical tomography can image spatial variations in highly scattering optical media; the multifrequency approach reported in this paper has great potential to substantially increase the quality of the images obtained by diffuse optical tomography systems; the technique developed as part of this research may also aid the development of new industrial applications where imaging through strongly scattering media is required.

REFERENCES

1. J. R. Mourant, T. Fuselier, J. Boyer, T. M. Johnson, and I. J. Bigio, *Predictions and measurements of scattering and absorption over broad wavelength ranges in tissue phantoms*, Appl.Opt., **39**, 949–957 (1997).
2. M. K. Nilsson, C. Sturesson, D. L. Liu, and S. Andersson-Engels, *Changes in spectral shape of tissue optical properties in conjunction with laser-induced thermotherapy*, Appl.Opt., **37**, *7*, 1256–1267 (1998).
3. H. Jiang, Y. Xu, N. Ifitimia, J. Eggert, K. Klove, L. Baron, and L. Fajardo, *Three dimensional optical tomography imaging of breast in a human subject*, IEEE Trans. Med. Imaging, **20**, 1334–1340 (2001).
4. B. W. Pogue, S. P. Poplack, T. O. McBride, W. A. Wells, K. S. Osterman, U. L. Osterberg, and K. D. Paulsen, *Quantitative hemoglobin tomography with diffuse near-infrared spectroscopy: Pilot results in the breast*, Radiology, **218**, 261–266 (2001).
5. B. W. Pogue, S. D. Poplack, T. O. McBride, S. Jiang, U. L. Osterberg, and K. D. Paulsen. *Breast tissue and tumour haemoglobin and oxygen saturation imaging with multi-spectral near infrared computed tomography*, Adv. Exp. Med. Biol., International Society on Oxygen Transport to Tissue Plenum Press Aug., 2001.
6. H.Wang, M. E. Putt, M. J. Emanuele, D. B. Shin, E. Glatstein, A. G. Yodh, and T. M. Busch, *Treatment-induced changes in tumor oxygenation predict photodynamic therapy outcome*, Cancer Res., **64**, 7553–7561 (2004).
7. J. C. Schotland, *Continuous-wave diffusion imaging*, J. Opt. Soc. Am., **A 14**, *1*, 275–279, 1997.
8. G. Gulsen, Bin Xiong, B. Oylem, and N. Orhan, *Design and implementation of a multifrequency near-infrared diffuse optical tomography system*, J. Of Biomedical Optics, **11**, *1*, 1–12, 1998.
9. Hiabei Jiang, Yong Xu, and Nicusor Iftimia, *Experimental three-dimensional optical image reconstruction of heterogeneous turbid media from continuous-wave data*, Optics Express, **7**, 204–209 (2000).
10. D. C. Dumitraş, D. C. Duţu, C. Matei, A. M. Măgureanu, M. Paţachia, *Diffuse optical tomography* (*DOT*) *with serial approach*, J. Optoelectron. Adv. Mater., – Symposia, **1**, 747–753 (2009).
11. M. Paţachia, D. C. A. Duţu, D. C. Dumitraş, Blood oxygenation monitoring by diffuse optical tomography, Quantum Electronics, **40**, 1062–1066 (2010).
12. M. Paţachia, *Calibration and artefact minimization in a two wavelength cw difuuse optical tomography system*, U.P.B. Sci. Bull., Series A, **75** (2013).
13. M. Paţachia, *A simple continuous-wave diffuse optical tomography system for parametric investigation of different tissue phantoms*, J. Optoelectron. Adv. Mater., **15**, 155–163 (2013).